photonics

MDPI

Article

A Highly Sensitive Plasmonic Graphene-Based Structure for Deoxyribonucleic Acid Detection

Zohre Salehnezhad [1], Mohammad Soroosh [1,*] and Haraprasad Mondal [2]

[1] Department of Electrical Engineering, Shahid Chamran University of Ahvaz, Ahvaz 61357, Iran; z-salehnezhad@stu.scu.ac.ir
[2] Department of Electronics and Communication Engineering, Dibrugarh University Institute of Engineering and Technology, Dibrugarh 786004, Assam, India; mondal.haraprasad@dibru.ac.in
* Correspondence: m.soroosh@scu.ac.ir; Tel.: +98-61-33226608

Abstract: In this study, a Kretschmann structure with a hybrid layer of graphene–WS_2 is designed to develop a sensitive biosensor for deoxyribonucleic acid detection. The biosensor incorporates a 45 nm gold layer as the active layer and a thin film of chrome as the adhesive layer. Through the optimization of the graphene and WS_2 layers, combined with the implementation of a silicon layer, we can enhance the nano-sensor's sensitivity. The thin silicon layer acts as a protective barrier for the metal, while also increasing the volume of interaction. Consequently, by adjusting the thickness of the active metal and adding a silicon layer, we achieve higher sensitivity and a lower full width at half maximum, leading to sensitivity of 333.33°/RIU. The designed structure is analyzed using numerical techniques and the finite difference time domain method, allowing us to obtain the optical characteristics of the surface plasmon polariton sensor. Various parameters are calculated and evaluated to determine the optimal conditions for the sensor. Furthermore, the total size of the sensor is 2.228 μm^2.

Keywords: biosensor; graphene; Kretschmann structure; sensitivity

Citation: Salehnezhad, Z.; Soroosh, M.; Mondal, H. A Highly Sensitive Plasmonic Graphene-Based Structure for Deoxyribonucleic Acid Detection. *Photonics* **2024**, *11*, 549. https://doi.org/10.3390/photonics11060549

Received: 12 May 2024
Revised: 6 June 2024
Accepted: 7 June 2024
Published: 9 June 2024

1. Introduction

Surface plasmon resonance (SPR) biosensors have garnered significant attention in cutting-edge research and play a crucial role in biosensing applications. These structures typically consist of an optical substrate coated with a thin metal layer, creating an ideal platform for the consideration of the analyte–biomolecule interaction [1–4]. Compared to traditional methods, these structures offer desirable advantages, including high sensitivity, versatility, real-time analysis, and label-free detection [5]. The attractive properties of graphene, such as light confinement at the graphene–dielectric interface, make it a suitable option to conduct surface plasmons in waveguides and sensors. Based on this, various devices have been designed, such as switches and decoders, encoders, and adders.

The operating principle of SPR is based on achieving resonance conditions, where the wave vector of the incident p-polarized light matches the wave vector of the surface plasmons. This leads to the excitation of surface plasmon waves (SPWs) at the metal–dielectric interface [6]. Consequently, a sharp dip in the light reflection curve is observed, indicative of surface plasmon resonance due to the conservation of energy and momentum from the incident light. To evaluate the sensor's performance, crucial factors such as the sensitivity and detection accuracy are assessed. Higher sensitivity implies superior performance, while the detection accuracy is inversely proportional to the full width at half maximum (FWHM) of the reflection curve. Therefore, a narrower reflection curve reduces the errors in calculating the resonance angle, resulting in improved detection accuracy [7].

In the selection of the optimal configuration to excite surface plasmons, the Kretschmann structure is preferred over the Otto configuration. In the Kretschmann structure, the metal layer is directly placed on the glass substrate (prism), without any intervening dielectric layer, unlike the Otto structure [8–11].

In addition to noble metals like gold and silver, which exhibit good sensitivity in surface plasmon resonance structures [12], two-dimensional materials such as graphene and tungsten disulfide (WS_2) have been proposed as alternatives to enhance the performance of SPR structures. These materials offer better cost-effectiveness and demonstrate superior performance. Graphene, for instance, can excite surface plasmon waves in the mid-infrared and terahertz frequency ranges. It also reduces the confinement of surface plasmon polaritons (SPPs) to a more reasonable level and exhibits a longer lifespan compared to metals [13]. Similarly, WS_2, another two-dimensional material, consists of a single layer of s-w-s atoms covalently bonded together and stacked with weak van der Waals bonds [14]. This material belongs to the category of 2D transition metal dichalcogenides and shows notable features, such as high photoresponsivity, a high density of electronic states, a wide band gap in the visible and mid-infrared range, and strong photoluminescence. WS_2 holds promise for the development of new chemical and biological sensors [15].

Numerous studies have been conducted on biosensors in plasmonic regimes, all aiming to enhance the performance of these biosensors. For example, Moradiani et al. presented a structure using polysilicon, silicon, gold, and graphene at terahertz wavelengths, achieving sensitivity of 45.14°/RIU [16]. Menon et al. employed graphene and MoS_2, along with a prism and a gold metal layer, at a wavelength of 633 nm [17]. Their biosensor demonstrated sensitivity of 130°/RIU, indicating that the addition of a graphene layer to the metal layer enhances the sensitivity. Building upon similar works at the same wavelength, Chabot et al. used WS_2 and WSe_2 materials and reported sensitivity of up to 142°/RIU [18]. A structure consisting of BK7–Au–WSe_2–$PESO_2$–BP layers was introduced, achieving sensitivity of 200°/RIU [14]. Moreover, a structure with BK7–MgO–Ag–BP layers demonstrated sensitivity of 234°/RIU [19].

Researchers have found that incorporating a high-refractive-index layer like silicon into the Kretschmann structure confines the plasmons between graphene and the analyte, resulting in an increased optical field and electron mobility on the graphene surface. These factors contribute to improved sensor performance. Additionally, varying the silicon thickness enables the adjustment of the working wavelength. In reference [20], a Kretschmann structure achieved sensitivity of 192°/RIU by incorporating silicon, graphene, and MoS_2 layers. The proposed work introduces a novel Kretschmann-based biosensor for biomolecule detection. A 65 nm thick silicon layer separates graphene and gold layers. By adding a WS_2 layer, the sensitivity of the designed sensor is increased to 333.33°/RIU, surpassing that in references [12,16–20]. The value of the FWHM is approximately 2.81°, making it applicable in sensor-based setups. Comparing the calculated FWHM to that in works [12,16–20] demonstrates the high performance of the proposed structure. The figure of merit is equal to 196.07 RIU^{-1}. The designed structure's area is approximately 2.228 μm^2. The obtained sensitivity facilitates biomolecule detection with the same indices for refraction. Furthermore, the designed structure holds potential for gas detection and biosensors. In this work, with the help of the silicon layer, which causes the greater confinement of the surface plasmons of graphene and the greater mobility of electrons in graphene, and also by using a hybrid layer of graphene and WS_2 and adjusting the number of layers of both of them, appropriate sensitivity and FWHM are achieved, offering enhanced capabilities for optical sensing applications and more accurate diagnosis compared to the reviewed references. The proposed structure has the potential to aid in the development of low-cost and efficient SPR-based biosensors, with a substantial shift in the resonance angle of the SPR curves.

Section 2 provides a detailed description of the proposed sensor. In Section 3, a comprehensive description of the theory is presented. The obtained results are reported and compared with those of similar structures in Section 4. Furthermore, the findings and a summary are presented in Section 4. Finally, Section 5 concludes the entire work.

2. The Proposed Structure

Figure 1 shows the proposed structure, referred to as a Kretschmann configuration, where six layers are stacked on a glass substrate. The layer sequence includes a BK7 prism, an adhesive layer composed of chrome, a silicon layer, a gold layer, graphene, tungsten disulfide, and a biosample, such as deoxyribonucleic acid. The structure is designed for light projection at an angle of θ and detection by a sensor. To achieve the resonance condition of light in this configuration, we utilize the BK7 prism with a refractive index (n_p) of 1.513 at a wavelength of 700 nm. The calculation of the np can be performed using the following formula [12]:

$$n_p = \left(1 + \frac{K_1\lambda^2}{\lambda^2 - K_2} + \frac{K_3\lambda^2}{\lambda^2 - K_4} + \frac{K_5\lambda^2}{\lambda^2 - K_6}\right)^{0.5} \quad (1)$$

where λ is the wavelength of incident light and it is equal to 700 nm. Coefficients K_1, K_2, K_3, K_4, K_5, and K_6 are equal to 1.03961212, 0.00600069867, 1.01044945, 103.60653, 0.231792344, and 0.0200179144, respectively. The graphene behaves dielectrically at a wavelength of 700 nm. This is a critical issue for surface plasmon polariton-based waveguides because the SPPs should be transmitted and controlled by the graphene layer. At a wavelength of 700 nm, the transmission loss becomes high, so it is not appropriate for the design of SPP-based devices such as encoders, decoders, and flip-flops. Due to the sensing operation of the proposed structure being performed in a small area, graphene can be used at the mentioned wavelength.

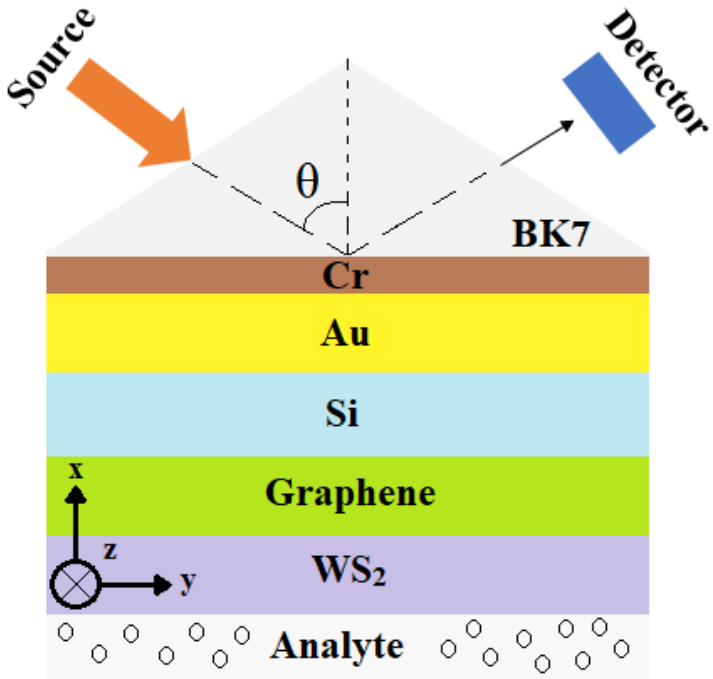

Figure 1. A two-dimensional view of the sensor's structure, including the Cr–Au–Si–graphene–WS_2 layers and the BK7 prism on top of the layers.

The Kretschmann configuration consists of a metal or graphene film deposited on a dielectric. A laser is coupled to the structure at a specific angle, known as the angle of total internal reflection. When the incident light hits the critical angle, surface plasmons are excited at the graphene–dielectric interface. These surface plasmons are sensitive to changes in the refractive index of the medium in contact with the graphene. When the medium in contact with the graphene changes—for example, due to the binding of biomolecules on the surface—the refractive index at the interface changes, leading to a shift in the surface

plasmon resonance angle. This shift can be detected by monitoring changes in the intensity of the reflected light or by measuring the angle of minimum reflectivity.

The sensitivity of the plasmonic sensor based on the Kretschmann structure is high because of the evanescent field interaction with the medium near the metal surface. This allows for the detection of small changes in the refractive index. Additionally, the specificity of the sensor can be enhanced by functionalizing the graphene surface with a recognition layer (such as WS_2) that selectively binds to the target analyte. Moreover, the absorption depth of silicon is approximately 8.3 μm for a wavelength of 700 nm, so the evanescent field in this study affects the light reflection. The absorption depth is the inverse of the absorption coefficient. The penetration depth of surface plasmon polaritons (δ) as a function of the wave vector (k) is as follows [21].

$$\delta = \frac{1}{k}\sqrt{\left|\frac{\varepsilon_{si} + \varepsilon_g}{-\varepsilon_{si}^2}\right|} \quad (2)$$

where ε_{si} and ε_g refer to the dielectric constants of silicon and graphene, respectively.

Table 1 provides the values of the refractive index and the thickness of the layers depicted in Figure 1 for a wavelength of 700 nm.

Table 1. The value of the refractive index and thickness for all layers shown in Figure 1.

Layer	Refractive Index		Thickness of Layer	
	Symbol	**Value (nm)**	**Symbol**	**Value (nm)**
Cr	n_{cr}	3.6 + 4.2i [12]	d_{cr}	0.5
Au	n_{Au}	0.13 + 4.06i [22]	d_{Au}	45
Si	n_{si}	3.7 + 0.012i [23]	d_{si}	65
Graphene	n_{Gr}	2.78 + 1.43i [24]	d_{Gr}	0.34
WS_2	n_{WS2}	4.05 + 0.11i [25]	d_{WS2}	0.65

The dielectric material, such as silicon, serves to enhance the excitation of SPPs at the graphene–dielectric interface by providing a medium with different permittivity from graphene. The permittivity mismatch between graphene and the dielectric can lead to the confinement and localization of the electromagnetic field at the interface, facilitating the excitation of SPPs. By choosing different dielectric materials with varying permittivity values, the properties of the SPPs at the graphene–dielectric interface can be tuned. The dielectric constant of the material affects the propagation length, dispersion relation, and energy confinement of the SPPs along the interface. The dielectric material can also help in reducing losses associated with SPP propagation. The proper selection of dielectric materials with low absorption in the desired spectral range can lead to the enhancement of the SPP propagation distances and the overall efficiency of the plasmonic devices.

Figure 2 shows the electric field distribution at the xy-plane for two cases: (a) with silicon and (b) without silicon. It can be inferred that the silicon layer helps to excite the surface plasmon polaritons at the graphene–silicon interface. By changing the refractive index of the analyte, the effective refractive index of the graphene is changed, and this affects the SPPs' excitation. Thus, the required incident angle for the excitation of SPPs changes. This feature determines the suitability of the structure for sensing operations.

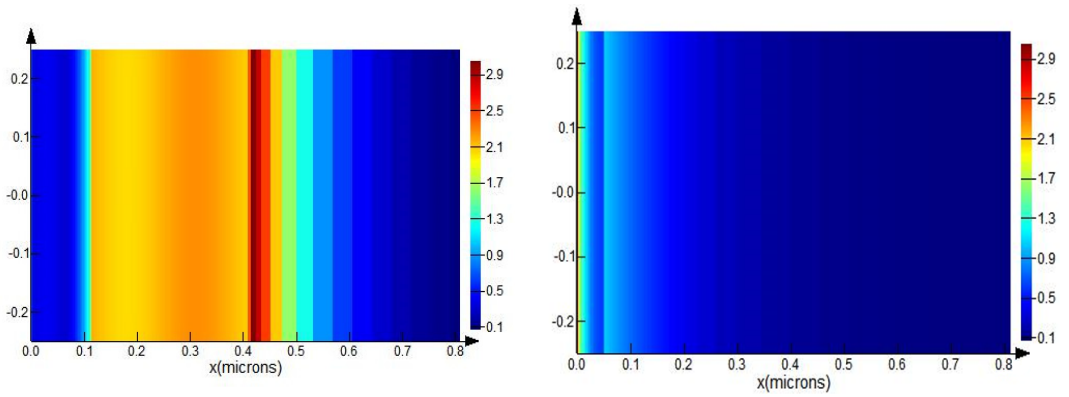

(**a**) (**b**)

Figure 2. The electric field distribution of the structure for two cases: (**a**) with silicon, (**b**) without silicon.

3. The Theory of Resonance

To achieve surface plasmon resonance between the metal and the dielectric interface, the wave vector of the surface plasmons (k_{sp}), defined by Equation (3), needs to be equal to the wave vector of the incident light (k_{in}) mentioned in Equation (4).

$$k_{sp} = \frac{\omega}{c}\sqrt{\frac{\varepsilon_g n_D^2}{\varepsilon_g + n_D^2}} \tag{3}$$

$$k_{in} = \frac{\omega}{c} n_p \sin\theta \tag{4}$$

where ω and c are the angular frequency and the speed of light, and n_D and ε_M represent the analyte and the gold's permittivity, respectively. The permittivity of graphene is defined as in Equation (5).

$$\varepsilon_g(\omega) = \varepsilon_{Si} + \frac{i\sigma_g(\omega)}{\omega\varepsilon_0\Delta} \tag{5}$$

where σ_g and Δ represent the conductivity and the effective thickness of graphene, respectively. The permittivity of the free space is shown by ε_0. Considering the resonance condition, $k_{sp} = k_{in}$ results in the required incident angle to excite the surface plasmon polaritons:

$$\theta_{sp} = \sin^{-1}\left(\frac{1}{n_p}\sqrt{\frac{\varepsilon_M n_D^2}{\varepsilon_M + n_D^2}}\right) \tag{6}$$

Equation (6) reveals that the refractive index of the analyzed analyte is affected by the angle of resonance. This means that as the analyte changes, the mentioned angle also varies. This property enables the sensing operation to be performed effectively [18].

In this study, the finite difference time domain (FDTD) technique is employed to solve Maxwell's equations. By utilizing this method, the electric and magnetic fields are calculated. The spatial cells in the x- and y-directions have a size of Δu = 2.5 nm, while the time cell is Δt = 8 as. The chosen cells meet Courant's condition, as stated in reference [26], ensuring the convergence of the simulations.

$$\Delta t \ll \frac{\Delta u}{c\sqrt{3}} \tag{7}$$

Moreover, the boundary conditions for the x-direction are implemented using the perfectly matched layer (PML), while the Bloch boundary condition is employed for the y-direction. By calculating the components of the magnetic and electric fields for all temporal and spatial cells, the interdependency among the meshes can be described as follows:

$$\begin{bmatrix} E_1 \\ H_1 \end{bmatrix} = M \begin{bmatrix} E_N \\ H_N \end{bmatrix} \tag{8}$$

where E_1 and H_1 represent the tangential components of the electric and magnetic fields at the first cell, while E_N and H_N represent the same components at the Nth layer, respectively. When incident light passes through the depicted layer, as shown in Figure 1, reflection occurs at each interface. The components of the M matrix correspond to the elements of a 2×2 matrix derived from the multiplication of matrices as described in reference [22]:

$$M = \prod_{j=1}^{j=N} M_j = \prod_{j=1}^{j=N} \begin{bmatrix} \cos p_j & \left(-i \sin p_j / q_j\right) \\ -i q_j \sin p_j & \cos p_j \end{bmatrix} = \begin{bmatrix} M_{11} & M_{12} \\ M_{21} & M_{22} \end{bmatrix} \tag{9}$$

where q_j and p_j are as follows:

$$q_j = \frac{\sqrt{\varepsilon_j - n_0^2 \sin^2 \theta}}{\varepsilon_j} \tag{10}$$

$$p_j = \frac{2\pi d j}{\lambda} \sqrt{n_j^2 - \sin^2 \theta} \tag{11}$$

The equations above involve several variables. N represents the number of cells and ε represents the permittivity. The index j corresponds to the cell index, while i represents the imaginary unit. In this context, d_j denotes the thickness of the layers, and n_0 represents the refractive index of air. From Equation (11), we can deduce that the characteristic matrix is influenced by both the refractive index and the layer thickness. Assuming that all layers are optically isotropic and non-magnetic, one can calculate the total reflection for p-polarized light using the following equation:

$$R = \left| \frac{\left(M_{11} + M_{12} q_N\right) q_1 - \left(M_{21} + M_{22} q_N\right)}{\left(M_{11} + M_{12} q_N\right) q_1 + \left(M_{21} + M_{22} q_N\right)} \right|^2 \tag{12}$$

4. Results and Discussion

Surface plasmon sensors often struggle in detecting biomolecules (such as deoxyribonucleic acid) at low concentrations and lightweight analytes. Enhancing the sensitivity to address this issue is a key focus of research in this field. To boost the sensitivity, various methods and solutions have been proposed. One such approach involves the placement of a high-index material such as silicon on the metal layer. This modification significantly improves the sensitivity by increasing θ_{sp} as the refractive index of the dielectric layer increases [23]. Consequently, the wave vector of surface plasmons (k_{sp}) increases, enhancing the sensitivity through an increased penetration depth.

The penetration depth of surface plasmons in the Kretschmann structure is inversely proportional to the wave vector. As the wave vector increases, the penetration depth decreases. This means that with higher wave vectors, the surface plasmons are confined more closely to the graphene–dielectric interface and do not penetrate as deeply into the dielectric medium. As a result, the interaction volume of the plasmons with the surrounding medium decreases, leading to enhanced surface sensitivity but a limited interaction depth. As the wave vector of the surface plasmons increases, the sensitivity of the Kretschmann structure also tends to increase. This heightened sensitivity is due to the tighter confinement of the plasmon wave along the interface between the graphene and the dielectric medium.

The deeper penetration is linked to a reduction in the k transverse component ($k_z = (k_x^2 - k_{sp}^2)^{0.5}$) due to the higher k_{sp} value. For instance, a silicon layer with a thickness of d_{si} = 65 nm is added onto the gold layer, as depicted in Figure 1. The optimization of this proposed biosensor involves adjusting the thickness of the silicon and metal layers, as well as the number of graphene and tungsten disulfide layers.

To study how the silicon layer impacts the sensor's performance, as depicted in Figure 3, sensitivity adjustments can be made by varying the thickness of the silicon layer. Thus, the thickness of the silicon layer was modified for this purpose. In Table 2, four different silicon thicknesses were tested, and the outcomes were analyzed. The results suggest that a thickness of d_{si} = 65 nm is an appropriate value. A laser source emitting light at a wavelength of 700 nm is directed at the BK7 prism from various angles. Concerning the refractive index of deoxyribonucleic acid (DNA), the analyte's index (n) equals either 1.55 or 1.553.

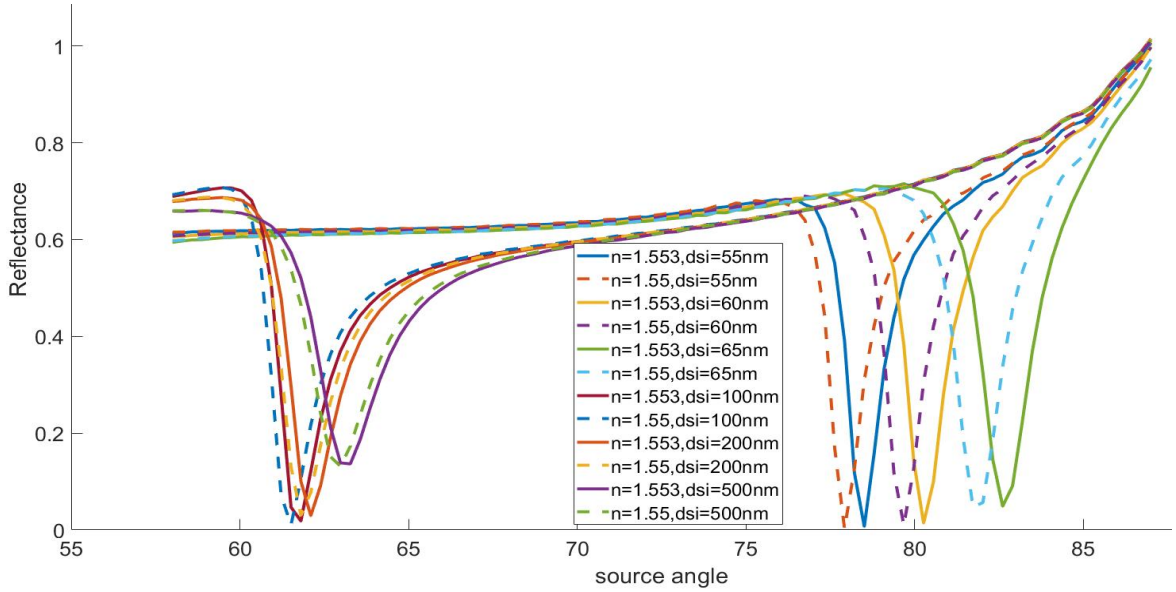

Figure 3. Detected light from the structure in terms of the source angles with an analyte refractive index of 1.55 and 1.553 for d_{Si} = 55, 60, 65, 100, 200, 500 nm.

Table 2. The calculated results for different thicknesses of the silicon layer.

dSi (nm)	θres (°)		S (°/RIU)	FWHM (°)	Dip
	n = 1.55	n = 1.553			
55	78.67	79.27	200	0.3	0.06
60	80.47	81.15	226.67	0.7	0.11
65	83.19	84.19	333.33	1.7	0.05
100	61.52	61.8	93.33	1.4	0.01
200	61.81	62.1	96.67	1.6	0.03
500	62.97	63.2	76.67	1.9	0.13

Figure 3 illustrates a shift in the resonance angle due to the change in refractive index, enabling the calculation of the sensitivity (S) and full width at half maximum. The resonance dip is defined as the reflected light for different resonance angles, which typically occurs at the minimum point of the figure. Additional simulation details are provided in Table 2.

In Table 2, it is apparent that for the optimally thick silicon layer in the structure, a minor variation in the analyte index (Δn = 0.003) yields S = 333.33°/RIU and FWHM = 1.7°. It has been shown that a critical factor influencing the SPR sensor's operation is the thickness of the metallic layer. In our investigation, we tested three different thicknesses of gold and compared their sensitivity and full width at half maximum, as detailed in Table 3. Additionally, Figure 4 displays the resonance angles for two samples with the index values of 1.553 and 1.55. From the results presented in Table 3, a thickness of 45 nm has been identified as the appropriate value for the gold layer.

Table 3. The calculated results of the sensor for different thicknesses of the gold layer.

d_{Au} (nm)	θ_{res} (°)		S (°/RIU)	FWHM (°)	Dip
	n = 1.55	n = 1.553			
40	79.72	80.32	200	1.37	0.01
45	83.19	84.19	333.33	1.7	0.15
50	83.11	84.01	296.67	1.9	0.3
55	81.91	82.75	280	1.1	0.25
60	81.98	82.80	273.33	1.2	0.35

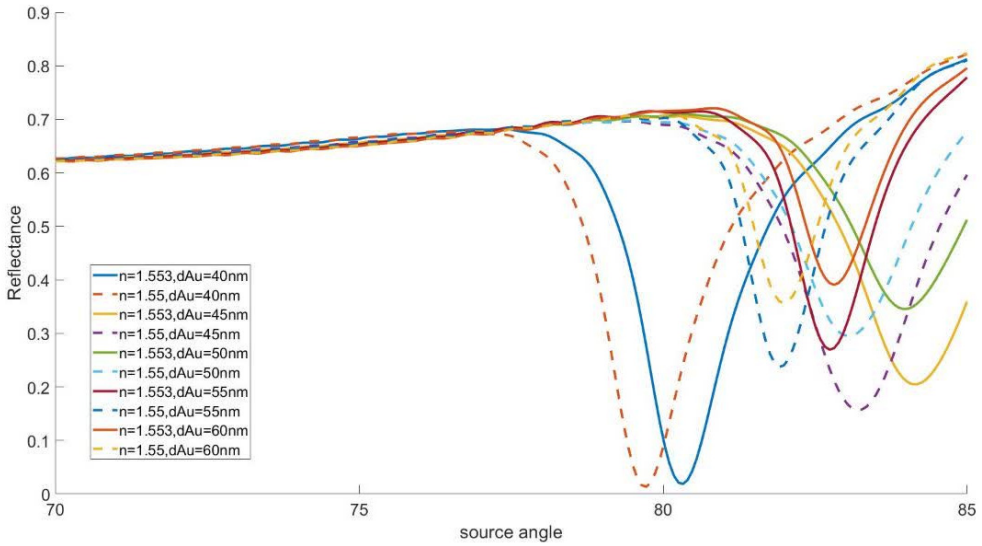

Figure 4. Reflectance from the structure versus the source angle for n = 1.55, 1.553 and d_{Au} = 40, 45, 50, 55, 60 nm.

In this research, tungsten disulfide layers are added onto graphene to enhance the results for the designed sensor. The thickness of a single layer of graphene and WS_2 is 0.34 nm and 0.8 nm, respectively. Figure 5 illustrates how the resonance angle shifts as the number of WS_2 layers changes from one to four for a single graphene layer. All of the layers considered exhibit nearly the same reflection values with varying θ_{sp}. While many of these angles could be chosen, the obtained results demonstrate that four graphene layers and four WS_2 layers, as well as the subsequent material layer, offer the most suitable configuration for further investigation and enhance the sensitivity of the structure. This finding is depicted in Figures 5–8, where the number of graphene layers ranges from one to four. These figures display the reflectance values concerning the incident angle for refractive indices of n = 1.55 and n = 1.553.

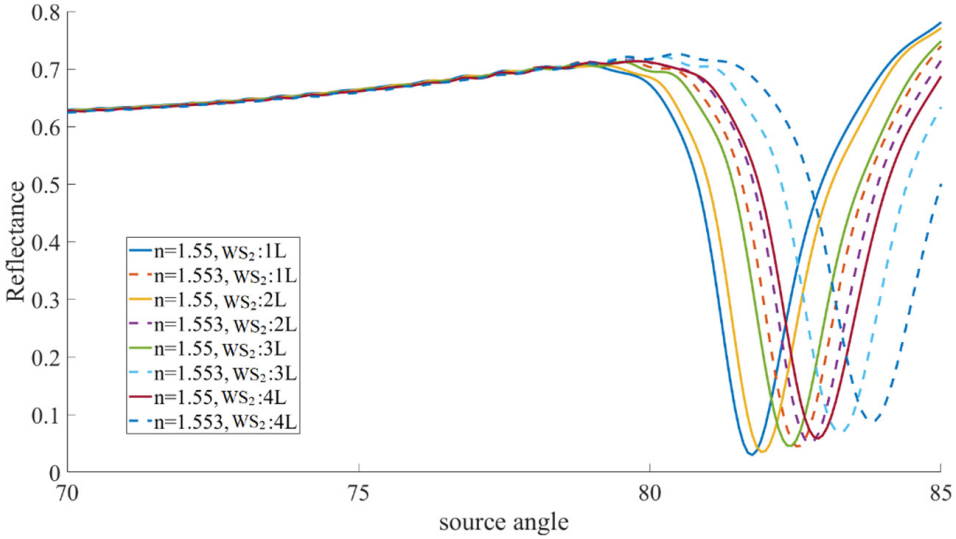

Figure 5. Reflection of the incident light in terms of the source angle for a single layer of graphene and 1 to 4 layers of WS_2 (1 L to 4 L). The refractive index of the analyte is 1.55 and 1.553.

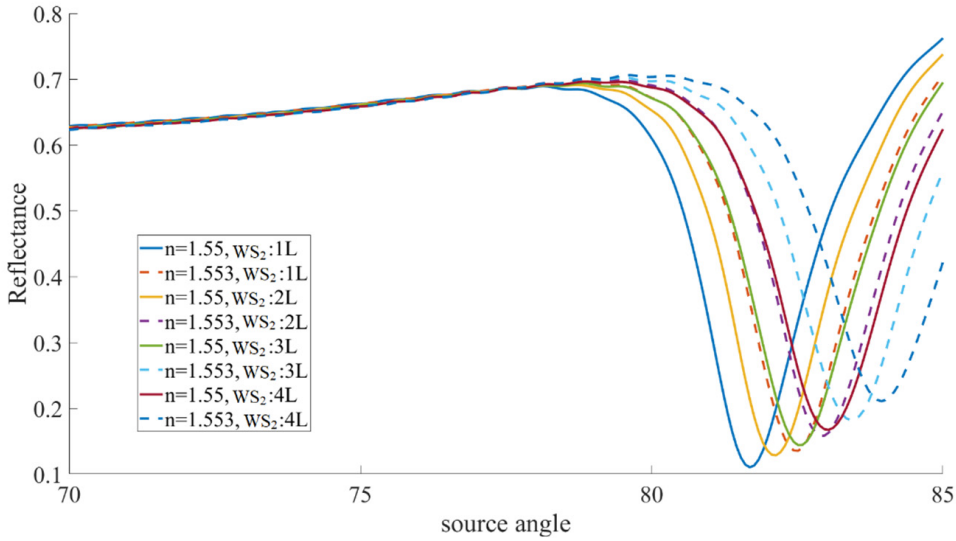

Figure 6. Reflection of the structure for different source angles and numbers of WS_2 layers (one layer to four layers). The structure includes two layers of graphene and the refractive index of the analyte is 1.55 and 1.553.

Table 4 displays the sensitivity of the structure as the number of graphene and WS_2 layers increases. It is evident that the device exhibits enhanced sensitivity with four graphene layers, and the sensitivity further improves for a greater number of WS_2 layers. The sensitivity values corresponding to one to three WS_2 layers are 276.67°/RIU, 303.33°/RIU, and 333.33°/RIU, respectively. However, the simulations indicate that adding another WS_2 layer (WS_2:4 L) decreases the sensitivity to 326.67°/RIU. Based on the aforementioned analysis, the optimal configuration for the current structure is as follows: prism/Cr (0.5 nm)/Au (45 nm)/Si (65 nm)/graphene (4 × 0.34 nm)/WS_2 (3 × 0.8 nm)/analyte. When the refractive index of the biosamples varies by 0.003, the resonance angle changes from 84.19° to 83.19°, as depicted in Figure 7. Therefore, the proposed biosensor can exhibit a shift of 1° at θ_{sp} for $\Delta n = 0.003$. The variation in the refractive index and the shift in θ_{sp} are listed in Table 5.

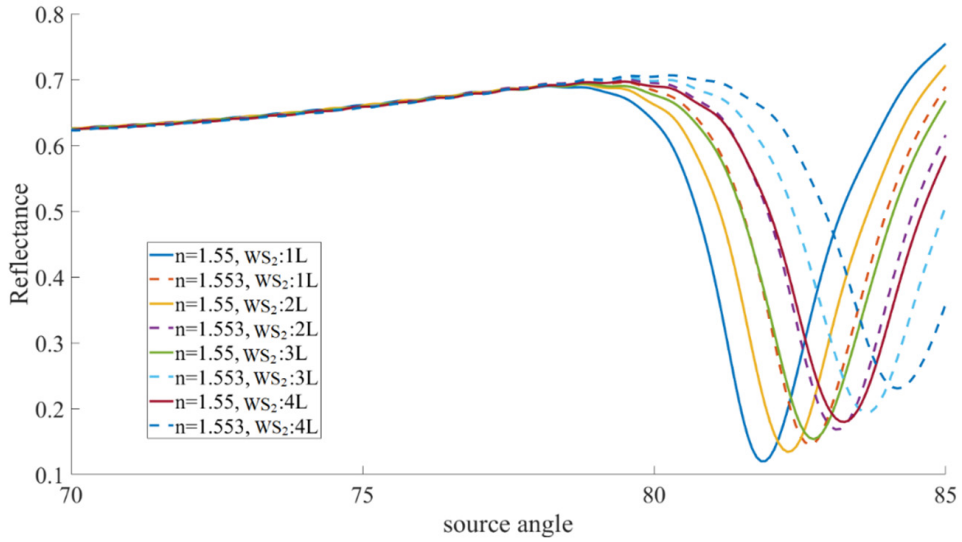

Figure 7. The reflection curve of the structure with three layers of graphene and a change in the number of WS_2 layers (1 L to 4 L) for n = 1.55, 1.553.

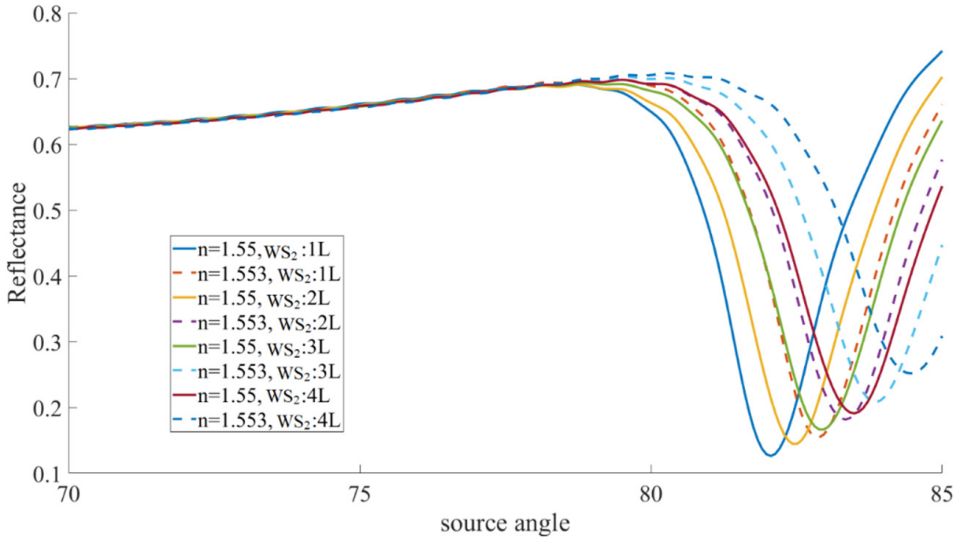

Figure 8. The reflectance in terms of the source angle with four layers of graphene and a change in the number of WS_2 layers. The analyte's refractive index is 1.55 and 1.553.

Table 4. The sensitivity of the proposed structure for different numbers of graphene and WS_2 layers.

Number of Graphene Layers	Sensitivity (°/RIU) for Number of WS_2 Layers			
	1	**2**	**3**	**4**
1	253.33	280	303.32	300
2	280	253.33	300	326.67
3	276.67	276.67	303.38	303.33
4	276.67	303.33	333.33	326.67

Figure 9 shows the electric field distribution of the structure for two cases: with graphene–WS_2 layers and without these layers. It can be inferred that the resonance in the graphene–silicon interface occurs at a depth of 0.11 µm and provides the strong confinement of the surface plasmon polaritons (as shown in Figure 9a). There is weaker resonance than the previous case at a depth of 0.045 µm, as shown in Figure 9b. The strong resonance at the

graphene–SiO_2 interface can help to achieve higher sensitivity. Changes in the refractive index of the analyte affect the required angle to achieve the resonance phenomenon. The sensitivity and the FOM for the structure including graphene–WS_2 layers are 333.33°/RIU and 196 1/RIU, respectively, while they are 29.7°/RIU and 21.2 1/RIU for the structure without graphene–WS_2 layers.

Table 5. The details of the obtained results for different numbers of graphene and WS_2 layers.

Number of Layers		θ_{res} (°)		S (°/RIU)	Dip
Graphene	WS_2	n = 1.55	n = 1.553		
1	1	81.75	82.51	253.33	0.03
	2	81.9	82.74	280	0.034
	3	82.36	83.27	303.33	0.045
	4	82.89	83.79	300	0.05
2	1	81.68	82.52	280	0.11
	2	82.13	82.89	253.33	0.12
	3	82.51	83.41	300	0.14
	4	82.96	83.94	326.67	0.16
3	1	81.83	82.66	276.67	0.12
	2	82.28	83.11	276.67	0.13
	3	82.73	83.64	303.33	0.15
	4	83.26	84.17	303.33	0.17
4	1	82.06	82.89	276.67	0.12
	2	82.43	83.34	303.33	0.15
	3	83.19	84.19	333.33	0.17
	4	83.49	84.47	326.67	0.19

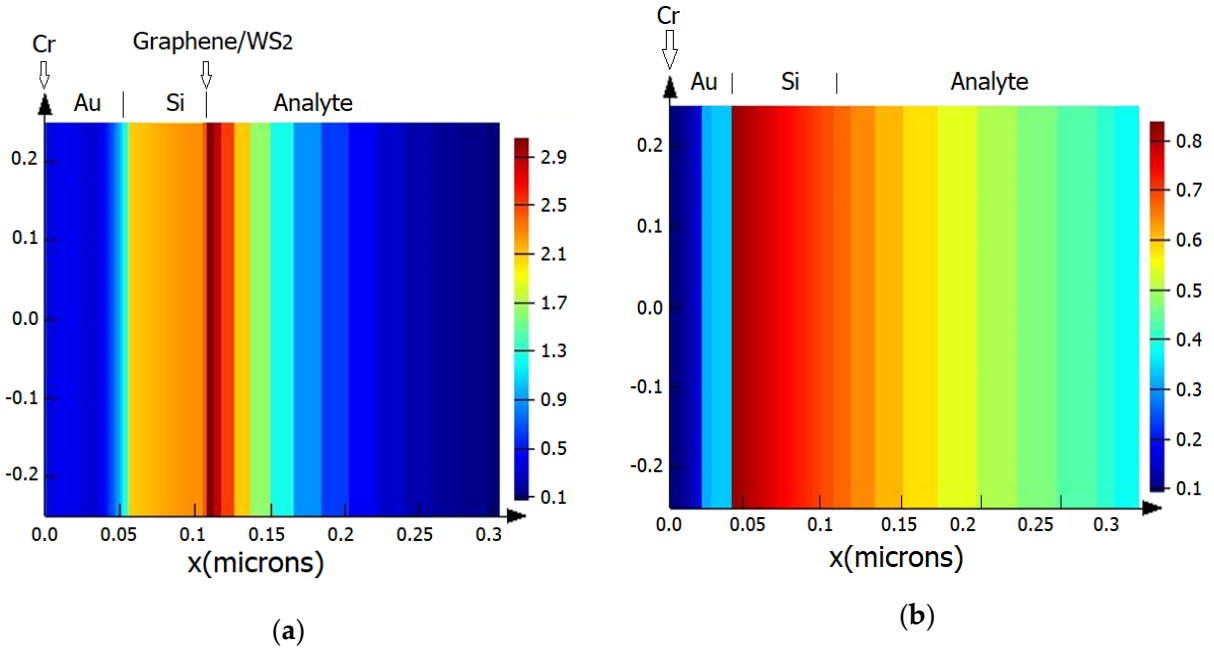

Figure 9. The electric field profile at the xz-plane (**a**) with graphene–WS_2 and (**b**) without graphene–WS_2.

As shown in Table 6, the obtained results, along with the results of others, are shown to evaluate the performance of this work. Moradiani et al. [16] and Parkayastha et al. [24] indicate that the structures presented need enhancements in terms of sensitivity. Wu et al. [25] demonstrate improved sensitivity; however, a sensor with higher sensitivity would outperform it, and the figure of merit of this structure could also be enhanced. Pandey et al. [12] and Jamil et al. [27] show significant improvements in sensitivity; nevertheless, the FOM remains low, signifying the necessity to enhance these structures. Salehnezhad et al. [20] introduce silicon, while reference [28] utilizes WS_2 layers to achieve better results. In this work, as indicated in Table 6, the obtained sensitivity has reached a suitable value, and the designed device exhibits a favorable figure of merit compared to other studies. Therefore, the presented structure can provide more precise detection and demonstrate higher sensing performance.

Table 6. The calculated results in contrast to other works.

Reference	Structure	Sensitive Materials	S (°/RIU)	FOM (1/RIU)	FWHM (°)
[16]	Graphene monolayer	Graphene	45.14	-	-
[24]	Otto	Graphene	34.11	1150	0.03
[25]	Kretschmann	Graphene	52	26	2
[17]	Kretschmann	Gold	94.51	15.19	7
[27]	Kretschmann	Graphene–MoS2	85.25	11.79	7.23
[20]	Kretschmann	Graphene–MoS2	192	68.32	2.81
[28]	Kretschmann	Graphene–WS2	288.86	88.89	3.24
This work	Kretschmann	Graphene–WS2	333.33	196	1.7

The discussion here focuses on the feasibility of fabricating a device structure. Initially, it is recommended to apply the Cr layer onto the glass substrate through EB evaporation [29]. The substrate undergoes ultrasonic cleaning in heated isopropanol and acetone before deposition [30]. Subsequently, the structure is layered with Si and Au using the CVD method [30]. For the deposition of the graphene layer, the chemical vapor deposition technique can also be utilized [31]. The growth of WS_2 on graphene may sometimes require extremely high temperatures. However, the growth of WS_2 on graphene at lower temperatures is feasible via the sulfurization of a tungsten precursor on graphene or by employing the plasma-enhanced atomic layer deposition method with $W(CO)_6$ and H_2S plasma [32]. The sensor structure is currently positioned on a rotating base, with a goniometer being utilized to adjust the resonance angle. Subsequently, monochromatic p-polarized light is directed onto one side of the prism, and the reflected light on the opposite side is captured by a photodetector. The reflection spectra obtained are then analyzed to ascertain the concentrations of the biomarkers present in the biological sample.

5. Conclusions

In this study, a highly sensitive surface plasmon resonance biosensor for deoxyribonucleic acid detection was developed utilizing a graphene–WS_2 hybrid layer, which influenced the field distribution within the sensing area and consequently enhanced the sensor's performance. By incorporating a high-refractive-index dielectric layer onto the metal, we enhanced the sensitivity of the SPR sensor. The high-index dielectric layer amplified the electric field at the interface between the dielectric and sensing medium, resulting in increased sensitivity compared to not having the dielectric layer. Moreover, improved sensitivity and performance were achieved by increasing the number of graphene and WS_2 layers. The findings from the calculations illustrated that the proposed structure significantly increased sensitivity up to 333.33°/RIU. The selected refractive indices for the

analyte and the structure's compatibility with fabrication technologies make the designed sensor promising for biosensor applications.

Author Contributions: Conceptualization, Z.S. and M.S.; methodology, Z.S.; software, Z.S.; validation, M.S. and H.M.; investigation, M.S. and H.M.; writing—original draft preparation, Z.S.; writing—review and editing, M.S. and H.M.; supervision, M.S.; project administration, M.S.; funding acquisition, M.S. All authors have read and agreed to the published version of the manuscript.

Funding: This work was supported by Shahid Chamran University of Ahvaz, grant number SCU.EE1402.672.

Institutional Review Board Statement: Not applicable.

Informed Consent Statement: Not applicable.

Data Availability Statement: All data generated or analyzed during this study are included in this published article.

Acknowledgments: The authors express their gratitude to Ali Basem and Hassan A. Kenjrawy for their cooperation in providing the high-speed processors for the simulation with the Lumerical software (version 2024).

Conflicts of Interest: The authors declare no conflicts of interest.

References

1. Jhaa, R.; Sharmab, A.K. Design of a silicon-based plasmonic biosensor chip for human blood-group identification. *Sens. Actuat. B* **2010**, *145*, 200–204. [CrossRef]
2. Salamon, Z.; Macleod, H.A.; Tollin, G. Surface plasmon resonance spectroscopy as a tool for investigating the biochemical and biophysical properties of membrane protein systems. I: Theoretical principles. *Biochim. Biophys. Acta* **1997**, *1331*, 117–124. [CrossRef] [PubMed]
3. Matveeva, E.; Malicka, J.; Gryczynski, I.; Gryczynski, Z.; Lakowicz, J.R. Multiwavelength immunoassays using surface plasmon-coupled emission. *Biochem. Biophys. Res. Commun.* **2004**, *313*, 721–726. [CrossRef] [PubMed]
4. Rajan, S.; Chand, B.D.; Gupta, D. Surface plasmon resonance based fiber-optic sensor for detection of pesticide. *Sens. Actuators B* **2007**, *123*, 661–666. [CrossRef]
5. Rakhshani, M.R.; Mansouri-Birjandi, M.A. Engineering hexagonal array of nanoholes for high sensitivity biosensor and application for human blood group detection. *IEEE Trans. Nanotechnoll.* **2018**, *17*, 475–481. [CrossRef]
6. Mohammadi, M.; Soroosh, M.; Farmani, A.; Ajabi, S. High-performance plasmonic graphene-based multiplexer/demultiplexer. *Diam. Relat. Mat.* **2023**, *139*, 110365. [CrossRef]
7. Farmani, A.; Mir, A.; Bazgir, M.; Zarrabi, F.B. Highly sensitive nano-scale plasmonic biosensor utilizing fano resonance metasurface in THz range: Numerical study. *Phys. E* **2018**, *104*, 233–240. [CrossRef]
8. Liedberg, B.; Nylander, C.; Lunström, I. Surface plasmon resonance for gas detection and bio-sensing. *Sens. Act.* **1983**, *4*, 299–304. [CrossRef]
9. Maier, S.A. *Plasmonics: Fundamentals and Applications*; Springer Science & Business Media: Berlin, Germany, 2007; pp. 123–143.
10. Kabashin, A.V.; Evans, P.; Pastkovsky, S.; Hendren, W.; Wurtz, G.A.; Atkinson, R.; Pollard, R.; Podolskiy, V.A.; Zayats, A.V. Plasmonic nanorod metamaterials for biosensing. *Nat. Mat.* **2009**, *8*, 867–871. [CrossRef]
11. Srivastava, T.; Purkayastha, A.; Jhaa, R. Graphene based surface plasmon resonance gas sensor for terahertz. *Opt. Quant. Electron.* **2016**, *48*, 334. [CrossRef]
12. Pandey, P.S.; Raghuwanshi, S.K.; Singh, R.; Kumar, S. Surface plasmon resonance biosensor chip for human blood groups identification assisted with silver-chromium-hafnium oxide. *Magnetochemistry* **2023**, *9*, 21. [CrossRef]
13. Maleki, M.J.; Soroosh, M. A low-loss subwavelength plasmonic waveguide for surface plasmon polariton transmission in optical circuits. *Opt. Quant. Electron.* **2023**, *55*, 1266. [CrossRef]
14. Ouyang, Q.; Zeng, S.; Jiang, L.; Hong, L.; Xu, G.; Dinh, X.Q.; Qian, J.; He, S.; Qu, J.; Coquet, P.; et al. Sensitivity enhancement of transition metal dichalcogenides/silicon nanostructure-based surface plasmon resonance biosensor. *Sci. Rep.* **2016**, *6*, 28190. [CrossRef]
15. Loh, T.A.; Chua, D.H.; Wee, A.T. One-step synthesis of few-layer WS2 by pulsed laser deposition. *Sci. Rep.* **2015**, *5*, 18116. [CrossRef] [PubMed]
16. Moradiani, F.; Farmani, A.; Yavarian, M.; Mir, A.; Behzadfar, F. A multimode graphene plasmonic perfect absorber at terahertz frequencies. *Phys. E Low-Dimens. Syst. Nanostructures* **2020**, *122*, 114159. [CrossRef]
17. Menon, P.S.; Gan, S.M.; Mohamad, N.R.; Jamil, N.A.; Tarumaraja, K.A.; Razak, N.R.; Bakar, A.A.A.; Mukhtar, W.M.; Murat, N.F.; Mohamed, R.; et al. Kretschmann based Surface Plasmon Resonance for Sensing in Visible Region. In Proceedings of the IEEE 9th International Nanoelectronics Conferences, Kuching, Malaysia, 3–5 July 2019; pp. 1–6.

18. Chabot, V.; Cuerrier, C.M.; Escher, E.; Aimez, V.; Geandbois, M.; Charette, P.G. Biosensing based on surface plasmon resonance and living cells. *Biosen. Bioelectron.* **2009**, *24*, 1667–1673. [CrossRef] [PubMed]
19. Aspnes, D.E.; Studna, A.A. Dielectric functions and optical parameters of Si, Ge, GaP, GaAs, GaSb, InP, InAs, and InSb from 1.5 to 6.0 eV. *Phys. Rev. B* **1983**, *27*, 985–1009. [CrossRef]
20. Salehnezhad, Z.; Soroosh, M.; Farmani, A. Design and numerical simulation of a sensitive plasmonic-based nanosensor utilizing MoS2 monolayer and graphene. *Diam. Relat. Mat.* **2023**, *131*, 109594. [CrossRef]
21. Zhang, J.; Zhang, L.; Xu, W. Surface plasmon polaritons: Physics and applications. *J. Phys. D Appl. Phys.* **2012**, *45*, 113001. [CrossRef]
22. Eng, Y.U.F.; Iu, Y.O.L. Design of an ultrasensitive SPR biosensor based on a graphene-MoS_2 hybrid structure with a MgF_2 prism. *Appl. Opt.* **2018**, *57*, 3639–3644.
23. Verma, R.; Gupta, B.D.; Jhaa, R. Sensitivity enhancement of a surface plasmon resonance based biomolecules sensor using graphene and silicon layers. *Sens. Actuat. B Chem.* **2011**, *160*, 623–631. [CrossRef]
24. Purkayastha, A.; Srivastava, T.; Jha, R. Ultrasensitive THz-Plasmonics gaseous sensor using doped graphene. *Sens. Actuators B Chem.* **2015**, *227*, 291–295. [CrossRef]
25. Wu, L.; Chu, H.S.; Koh, W.S.; Li, E.P. Highly sensitive graphene biosensors based on surface plasmon resonance. *Opt. Exp.* **2010**, *18*, 14395–14400. [CrossRef] [PubMed]
26. Maleki, M.J.; Soroosh, M.; Akbarizadeh, G. A subwavelength graphene surface plasmon polariton-based decoder. *Diam. Relat. Mat.* **2023**, *134*, 109780. [CrossRef]
27. Jamil, N.A.; Gan, S.M.; Khairulazdan, N.B.; Thiagarajah, S.P.; Hamzah, A.A.; Majlis, B.Y.; Menon, P.S. Detection of uric acid using Kretschmann-based SPR biosensor with MoS2-graphene. In Proceedings of the IEEE Student Conference on Research and Development, Selangor, Malaysia, 26–28 November 2018; pp. 1–4.
28. Yadav, A.; Mishra, M.M.; Tripathy, S.K.; Kumar, A.; Singh, O.P.; Sharan, P. Improved surface plasmon effect in Ag-based SPR biosensor with graphene and WS2:an approach towards low cost Urine-glucose detection. *Plasmon* **2023**, *18*, 2273–2283. [CrossRef]
29. Saeidifard, S.; Sohrabi, F.; Ghazimoradi, M.H.; Mehri Hamidi, S.; Farivar, S.; Ansari, M.A. Two-dimensional plasmonic biosensing platform: Cellular activity detection under laser stimulation. *J. Appl. Phys.* **2019**, *126*, 104701. [CrossRef]
30. Wu, F.; Singh, J.; Thomas, P.; Ge, Q.; Kravets, V.; Day, P.J.; Grigorenko, A.N. Ultrasensitive and rapid detection of malaria using graphene-enhanced surface plasmon resonance. *2D Mat.* **2020**, *7*, 045019. [CrossRef]
31. Jussila, H.; Yang, H.; Granqvist, N.; Sun, Z. Surface plasmon resonance for characterization of large-area atomic-layer graphene film. *Optica* **2016**, *3*, 151. [CrossRef]
32. Yeo, S.; Nandi, D.K.; Rahul, R.; Kim, T.H.; Shong, B.; Jang, Y.; Bae, J.S.; Han, J.W.; Kim, S.H.; Kim, H. Low-temperature direct synthesis of high quality WS2 thin films by plasma-enhanced atomic layer deposition for energy related applications. *Appl. Surf. Sci.* **2018**, *459*, 596–605. [CrossRef]